CHAPTER 1

LOCAL LINEAR STABILITY ANALYSIS

1.1 INTRODUCTION

Until the advent of high performance computers, local stability analysis was the standard approach to flow instability. These days it is still useful although, as computers become more powerful, it is likely to be used more as a diagnostic tool than as a predictive tool. Nevertheless, its speed makes it well-suited to problems at high Reynolds numbers and in complex geometry, for which global stability analysis is very computationally expensive.

This chapter explains the methodology behind local stability analysis and then contains some worked examples in Matlab. These introduce the concepts of phase and group velocity, temporal analyses, spatial analyses, Gaster's transformation, spatio-temporal stability analyses and how to re-construct a global mode from a local analysis.

1.2 METHODOLOGY

We take a steady flow, known as the *base flow*, and investigate the behaviour of infinitesimal perturbations to that flow. These perturbations are governed by the linearized Navier–Stokes equation (LN–S), which is derived in section 1.3. This equation has three dimensions in space and one in time. The time dimension is usually semi-infinite, *i.e.* it starts at $t = 0$ and 'ends' at $t = \infty$. This means that a Fourier decomposition is appropriate, *i.e.* we consider solutions of the form $\mathbf{u}(x, y, z)\exp(-\mathrm{i}\omega t)$ and then integrate over all ω. For most

values of ω, the only permitted solution is $\mathbf{u}(x, y, z) = 0$. For some values of ω, however, the LN–S equation and boundary conditions permit non-zero solutions of $\mathbf{u}(x, y, z)$. These values of ω are the *eigenvalues* of the system and the corresponding fields $\mathbf{u}(x, y, z)$ are their *eigenfunctions*. Together, they are called the *eigenmodes* or *global modes*. Usually we consider just the eigenmode with the highest growth rate and do not perform the integration in ω.

In general, the eigenfunctions $\mathbf{u}(x, y, z)$ are three-dimensional. It is possible to calculate three-dimensional eigenfunctions but it is very computationally expensive. If the base flow is planar (*i.e.* invariant in the y direction) or axisymmetric (*i.e.* invariant in the θ direction) then another Fourier decomposition can be performed in, respectively, the cross-stream direction , $\exp(\mathrm{i}k_y y)$, or the azimuthal direction, $\exp(\mathrm{i}m\theta)$. This reduces the three-dimensional eigenvalue problem to a set of two-dimensional eigenvalue problems for $\tilde{\mathbf{u}}(x, z)$.

It is possible to calculate two-dimensional eigenfunctions but it is still computationally expensive and, until recently, was impractical. If the base flow is planar or axisymmetric and also invariant in the streamwise (x) direction then a further Fourier decomposition can be performed in the x-direction, $\exp(\mathrm{i}kx)$. This reduces the two-dimensional eigenvalue problem to a set of one-dimensional eigenvalue problems for $\hat{\mathbf{u}}(z)$. These can be calculated very quickly numerically and, for some flows, can even be calculated analytically.

Of course, most real flows are not invariant in the streamwise direction because of the action of viscous forces. A more rigorous analysis, therefore, needs to consider the streamwise dependence of perturbations as the product of a function that varies on a fast streamwise lengthscale and another function that varies on a slow streamwise lengthscale. This is the *WKBJ* approximation. This approximation is justifiable as long as the base flow varies on a much longer lengthscale than the wavelength of the perturbations. Using an axisymmetric base flow as an example, we take the axial and azimuthal velocity profiles at each streamwise location and stretch them to infinity in the streamwise direction. (We have to set the radial velocity to zero in order to satisfy continuity.) Then we examine each slice separately. Reviews by [Huerre & Monkewitz (1990)] and [Huerre & Monkewitz (2000)] and the paper by [Monkewitz, Huerre & Chomaz (1993)] describe this process formally and in great detail. It is analogous to the two-timing approach to nonlinear problems that evolve on two different timescales [Strogatz (2001)].

This reduction of a three-dimensional problem to a set of one-dimensional problems is the basis for the *local stability analysis* of *open* shear flows. Local stability analysis is very quick and sometimes remarkably accurate. These days, it is best used in conjunction with global stability analysis because it provides useful information about the base flow that cannot be obtained from a global analysis alone.

1.3 LINEARIZATION AND FOURIER DECOMPOSITION

The N–S equation and incompressibility condition are:

$$\frac{\partial \mathbf{U}}{\partial t} + \mathbf{U} \cdot \nabla \mathbf{U} = -\nabla P + \frac{1}{Re} \nabla^2 \mathbf{U}, \tag{1.1}$$

$$\nabla \cdot \mathbf{U} = 0. \tag{1.2}$$

The base flow is assumed to be a steady solution to (1.1) – *i.e.* it satisfies (1.1) when the time derivative term is zero. The velocity and pressure are expressed as a sum of the base flow components and the infinitesimal perturbation components, such that $\mathbf{U} = \bar{\mathbf{U}} + \epsilon\mathbf{u}$ and $P = \bar{P} + \epsilon p$, where ϵ is small. These are substituted into (1.1) and then the steady solution corresponding to the base flow is subtracted. The linearized Navier–Stokes equation is then given by the highest order terms, which are all first order in ϵ:

$$\frac{\partial \mathbf{u}}{\partial t} + \mathbf{u}\cdot\nabla\bar{\mathbf{U}} + \bar{\mathbf{U}}\cdot\nabla\mathbf{u} = -\nabla p + \frac{1}{Re}\nabla^2\mathbf{u}, \tag{1.3}$$

$$\nabla\cdot\mathbf{u} = 0. \tag{1.4}$$

Terms in higher orders of epsilon (in this case they are all in ϵ^2) are neglected. This is a set of four partial differential equations (PDEs) in four unknown functions, (u, v, w, p), each defined in three spatial dimensions, x, y, z, and one time dimension, t.

Now we perform the Fourier decompositions in x, y, and t by substituting $\mathbf{u}(x, y, z, t) = \hat{\mathbf{u}}(z)\exp\{\mathrm{i}(kx + k_y y - \omega t)\}$ and $p(x, y, z, t) = \hat{p}(z)\exp\{\mathrm{i}(kx + k_y y - \omega t)\}$. This reduces the four PDEs for four functions in four dimensions to four Ordinary Differential Equations (ODEs) for four unknown functions $(\hat{u}, \hat{v}, \hat{w}, \hat{p})$, in one dimension, z. These governing equations, together with boundary conditions for the unknown functions, comprise a one-dimensional eigenvalue problem. In other words, for specified values of k and k_y, the governing equations and boundary conditions can only be satisfied for certain values of ω.

The governing equations can be solved simultaneously. (This is often the best way because it uses only first derivatives in the base flow velocity profile and is therefore less susceptible to errors.) Alternatively, the four unknown functions can be reduced to one unknown function, and the four equations reduced to one equation through substitution; [Drazin & Reid (1981)] §25. A convenient trick in two spatial dimensions (*i.e.* with $k_y = 0$) is to eliminate $\hat{p}$ by substitution and then to solve for the streamfunction $\psi = \hat{\psi}(z)\mathrm{e}^{\mathrm{i}kx}$ instead: $\hat{u} = \partial\hat{\psi}/\partial z$, $\hat{w} = -\mathrm{i}k\hat{\psi}$. This leads to the Orr-Sommerfeld (O–S) equation:

$$\frac{1}{\mathrm{i}kRe}\left(\frac{\mathrm{d}^2}{\mathrm{d}z^2} - k^2\right)^2\hat{\psi} = \left(U - \frac{\omega}{k}\right)\left(\frac{\mathrm{d}^2}{\mathrm{d}z^2} - k^2\right)\hat{\psi} - \frac{\mathrm{d}^2 U}{\mathrm{d}z^2}\tilde{\psi}. \tag{1.5}$$

It is easy to check that this equation is of the Sturm–Liouville type and therefore admits solutions only for certain eigenvalue pairs of (ω, k).

The analysis in two spatial dimensions is particularly common because we know from *Squire's theorem* that, for a planar flow in one direction, the two-dimensional eigenmodes are always more unstable than their three-dimensional counterparts; [Drazin & Reid (1981)] §25. In other words, the most unstable eigenmodes always have $k_y = 0$. Unfortunately, this convenient trick masks the fact that three-dimensional perturbations tend to give rise to the maximum *transient* growth, even though they do not have the maximum *long term* (*i.e.* eigenvalue) growth.

The governing equations and boundary conditions, whether as four separate equations or one single equation, are usually solved numerically with shooting methods or spectral methods. Shooting methods are easier to understand but spectral methods are easier to implement. Nick Trefethen's book *Spectral Methods in Matlab* is an excellent tutorial,

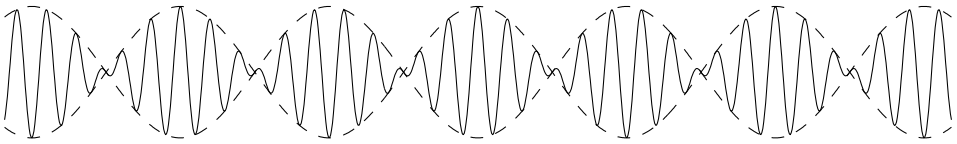

Figure 1.1. Waves often travel in packets and have a well-defined envelope. The phase velocity is the velocity at which the wave crests travel. The group velocity is the velocity at which the envelope travels.

with accompanying Matlab scripts, and contains a Chebyshev method that solves the O–S equation.

Spectral methods express the governing equations and boundary conditions as a generalized matrix eigenvalue problem of the form

$$\mathbf{A}(k)\psi = \omega\mathbf{B}(k)\psi. \tag{1.6}$$

For each k, the permitted values of ω are found by solving this matrix eigenvalue problem. For some base flows, it is possible to derive an analytical relationship for $\omega(k)$. Whether expressed as a generalized matrix eigenvalue problem or as an analytical expression, the relationship between permitted values of ω and k is called the *dispersion relation*, for reasons explained in the next section.

1.4 PHASE VELOCITY AND GROUP VELOCITY

The Fourier variables k and ω have important physical relevance. The perturbations can be written as $\mathbf{u}(x,z,t) = \hat{\mathbf{u}}(z)\mathrm{e}^{\mathrm{i}k_r x}\mathrm{e}^{-k_i x}\mathrm{e}^{-\mathrm{i}\omega_r t}\mathrm{e}^{\omega_i t}$. By considering how each of the four exponential terms behaves as x and t increase, it is easy to see that the perturbations are wave-like and that k_r is $2\pi/\lambda$, where λ is the streamwise wavelength, k_i is the decay rate in space of the envelope of the waves, ω_r is the angular frequency of the waves, and ω_i is the growth rate in time of the envelope of the waves.

The perturbations can also be written as $\mathbf{u}(x,z,t) = \hat{\mathbf{u}}(z)\exp\{\mathrm{i}k(x-ct)\}$, where $c \equiv \omega/k$. For a given k, the value of $\mathbf{u}$ is therefore constant along a particular ray with $(x - ct)$ = constant. In other words, c is the velocity of the wave crests, which is known as the *phase* velocity. If (and only if) ω is directly proportional to k, then every wavenumber has the same phase velocity and the medium is known as a *non-dispersive* medium.

In general, the perturbation consists of a superposition of many waves, which interfere with each other constructively and destructively. The patterns of constructive and destructive interference usually cause the perturbation to have an identifiable envelope, as shown in figure 1.1.. If the wavecrests of all wavenumbers move at the same phase velocity, then this interference pattern, and therefore this envelope, also move at the phase velocity and they do not change shape over time. If, however, the wavecrests of different wavenumbers move at different phase velocities, then this interference pattern changes shape over time and the envelope moves at a different velocity to the wave crests. The velocity of the envelope is known as the *group* velocity and it is equal to $\mathrm{d}\omega/\mathrm{d}k$. In this case, the medium is

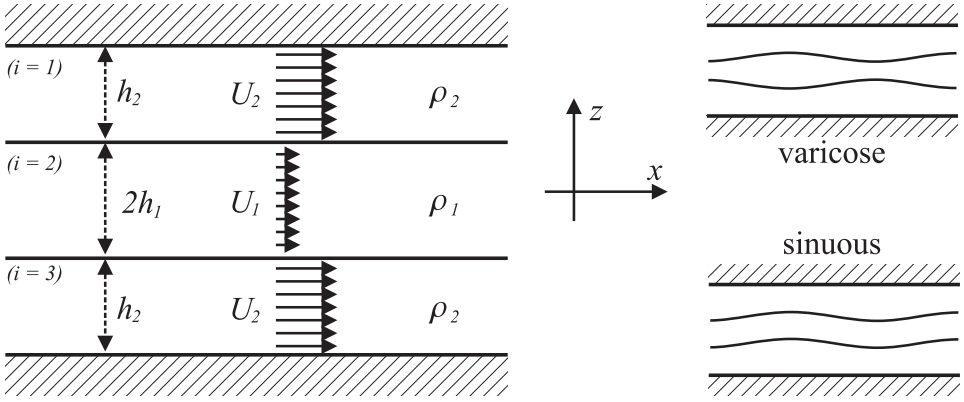

Figure 1.2. The base flows in this tutorial are all planar jets and wakes with top hat velocity profiles. These flows have analytical dispersion relations, which can be calculated without spectral or shooting methods.

known as a *dispersive* medium.

Perhaps surprisingly, the group velocity has more physical relevance than the phase velocity. This is because it is the velocity at which energy and information travel. For example, light travels at 3×10^8 ms^{-1} in a vacuum. A vacuum is a non-dispersive medium, so the phase velocity equals the group velocity. Condensed matter is a dispersive medium, however, so outside a vacuum the phase velocity of light does not equal the group velocity. In fact, the phase velocity of light outside a vacuum is greater than 3×10^8 ms^{-1} (!), but fortunately the group velocity, which is the speed at which information travels, is less than 3×10^8 ms^{-1}. The distinction between phase and group velocity is one of the most important concepts in local stability analysis and we will return to it repeatedly.

1.5 THE DISPERSION RELATIONS FOR SIMPLE FLOWS

Most analyses of local stability are performed by solving the O–S equation numerically using spectral methods in one dimension. Before such methods were available, dispersion relations for a few simple flows were derived analytically. These dispersion relations are used in this chapter because their qualitative behaviour is much the same as that of the O–S equation, but they are easier to derive, understand, manipulate, and analyse. They have come from [Rayleigh (1896)] §§365 – 369, [Drazin & Reid (1981)] §§4–5, [Yu & Monkewitz (1990)] and [Juniper (2007)] They are expressed in dimensionless form in the format preferred by [Huerre & Monkewitz (2000)]: as a function that equals zero: $D \equiv f(\omega, k) = 0$. It is easiest to explain the flow with the most features first and then simplify it by removing the features one by one.

The flow with the most features is shown in figure 1.2.. It is a planar flow consisting of a central flow with density ρ_1, velocity U_1 and width $2h_1$, surrounded by two flows with density ρ_2, velocity U_2 and width h_2. The velocities and densities are uniform except at the shear layers between the fluids, where they jump discontinuously across an interface that has surface tension σ. We will consider only varicose perturbations, in which the shear

layers move in opposite directions, and sinuous perturbations, in which the shear layers move in the same direction. Any perturbation can be expressed as a linear combination of a varicose and sinuous perturbation. The dimensionless parameters are

- the shear ratio $\Lambda \equiv (U_1 - U_2)/(U_1 + U_2)$;
- the density ratio $S \equiv \rho_1/\rho_2$;
- the confinement ratio h_2/h_1;
- the surface tension $\Sigma \equiv 4\sigma/(h_1\rho_2(U_1 + U_2)^2)$.

Various symmetries in the model become more apparent if a slightly different set of reference scales and dimensionless parameters are used [Rees & Juniper (2009)], but the dispersion relations become less easy to read.

The dispersion relations are

- varicose perturbations of a confined planar jet/wake

$$D \equiv S(1 + \Lambda - \omega/k)^2 \coth(\xi) + (1 - \Lambda - \omega/k)^2 \coth(\xi h) - \xi\Sigma = 0 \qquad (1.7)$$

- sinuous perturbations of a confined planar jet/wake

$$D \equiv S(1 + \Lambda - \omega/k)^2 \tanh(\xi) + (1 - \Lambda - \omega/k)^2 \coth(\xi h) - \xi\Sigma = 0 \qquad (1.8)$$

- varicose perturbations of an unconfined planar jet/wake

$$D \equiv S(1 + \Lambda - \omega/k)^2 \coth(\xi) + (1 - \Lambda - \omega/k)^2 - \xi\Sigma = 0 \qquad (1.9)$$

- sinuous perturbations of an unconfined planar jet/wake

$$D \equiv S(1 + \Lambda - \omega/k)^2 \tanh(\xi) + (1 - \Lambda - \omega/k)^2 - \xi\Sigma = 0 \qquad (1.10)$$

- perturbations of an unconfined single shear layer

$$D \equiv S(1 + \Lambda - \omega/k)^2 + (1 - \Lambda - \omega/k)^2 - \xi = 0 \qquad (1.11)$$

  ($\Sigma = 1$ for an unconfined single shear layer because the surface tension defines the reference lengthscale h_1)

The variable ξ is required in order to keep branch points off the k_r axis, as described in [Healey (2006)] and [Juniper (2007)]. It is given by $\xi \equiv +(k^2 + k_y^2)^{1/2}$ as $k_y \to 0$. Here, however, we shall examine only $k \geq 0$ and therefore ξ can be replaced by k.

Surface tension is required in order to prevent ω from becoming infinite as k becomes infinite. Surface tension has a strong effect on absolute instability, however, as described in [Rees & Juniper (2009)]. An alternative strategy is to introduce a finite shear layer thickness. This prevents ω from becoming infinite and has only a mild effect on long wavelength instabilities. Analytical dispersion relations exist for the analogous flows [Juniper (2007)].

1.6 CODING THE DISPERSION RELATIONS

It is quite easy (but rather tedious) to use the quadratic formula to derive $c \equiv \omega/k$ as an analytic function of k. It is quicker to use Matlab functions. The function `fun_eval_c_single.m` evaluates the two values of c for a given value of k. It uses the quadratic formula and then uses a stencil to change Matlab's default ordering of `c1` and `c2`. (The stencil does not become important until we consider the spatio-temporal analysis in section 1.11.)

The function has been constructed so that entire arrays of `c1` and `c2` can be calculated simultaneously. This requires operators such as $(.\star)$ to be used instead of $(\star)$. The parameters Λ and S are held in a Matlab structure as `param.L` and `param.S`. This notation makes it easy for a single script to call a variety of functions.

1. Write Matlab functions to calculate ω/k for the remaining dispersion relations. Name them
   - `fun_eval_c_unconf_jetwake_sin.m`
   - `fun_eval_c_unconf_jetwake_var.m`
   - `fun_eval_c_conf_jetwake_sin.m`
   - `fun_eval_c_conf_jetwake_var.m`
2. Try calling these functions with the generic functions `fun_eval_c.m` and `fun_eval_w.m` in order to become familiar with the program structure.
3. With the exception of the single shear layer, iterative procedures are required in order to find k as a function of ω. These involve setting the function D to zero by changing k at given ω. Write Matlab functions to calculate D for each dispersion relation, given ω and k. Name them
   - `fun_eval_D_single.m`
   - `fun_eval_D_unconf_jetwake_sin.m`
   - `fun_eval_D_unconf_jetwake_var.m`
   - `fun_eval_D_conf_jetwake_sin.m`
   - `fun_eval_D_conf_jetwake_var.m`
4. Try calling these functions with the generic function `fun_eval_D.m`.
5. Write a script that calculates ω using the first set of functions and then checks that this (ω, k) pair satisfies $D = 0$ by calling the second set of functions.

These functions will be the building blocks for rest of this tutorial.

1.7 TEMPORAL STABILITY ANALYSIS

In a temporal stability analysis, we constrain k to be a real number. Physically, this means that we consider only waves that do not grow or decay in the streamwise direction. We then ask whether such waves grow or decay in time. An example is shown in figure 1.3. (left) for a single shear layer with $\Lambda = 0.9$ and $S = 1$.

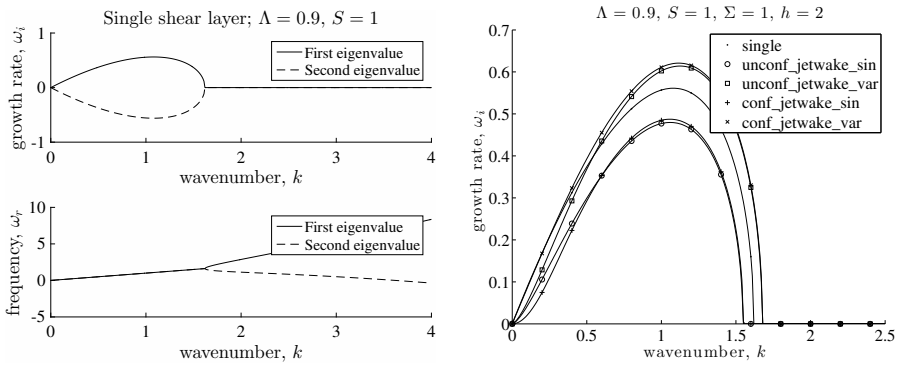

Figure 1.3. Left: the real and imaginary components of $\omega(k)$ calculated with a temporal stability analysis, in which k is constrained to be real. Right: the imaginary components of $\omega(k)$ for the five dispersion relations.

1. Write a script called `script_temporal_001.m` to generate figure 1.3. (left).
2. There are two regimes, either side of $k = 1.6$. How do the waves behave in these two regimes?
3. Vary Λ and S to see how this model behaves.
4. Write a script called `script_temporal_002.m` to perform the temporal analysis on all the dispersion relations and to plot their growth rates as a function of positive k on the same plot, as shown in figure 1.3.(right).
5. What do you observe? In particular, how does confinement affect the temporal stability of the flows?

1.8 GROUP VELOCITY

The phase velocity $c \equiv \omega/k$ is the velocity of wavecrests. The group velocity $c_g \equiv \mathrm{d}\omega/\mathrm{d}k$ is the velocity of wavepackets. In a dispersive medium, $c \neq c_g$.

1. Write a function called `fun_eval_dwdk.m` to evaluate the group velocity as a function of k. A first order finite difference method will be good enough.
2. Write a script called `script_groupvel_001.m` to compare the phase and group velocities as shown in figure 1.4..
3. Investigate the different dispersion relations at different parameter values. What do you observe? Look particularly at unconfined low density jets ($\Lambda \sim 1, S \ll 1$) at small values of Σ.

1.9 SPATIAL STABILITY ANALYSIS

In a spatial stability analysis, we constrain ω to be a real number. Physically, this means that we force sinusoidally at a particular point in space and see whether the resulting perturbations grow (negative k_i) or decay (positive k_i) in space. This is known as the *signalling*

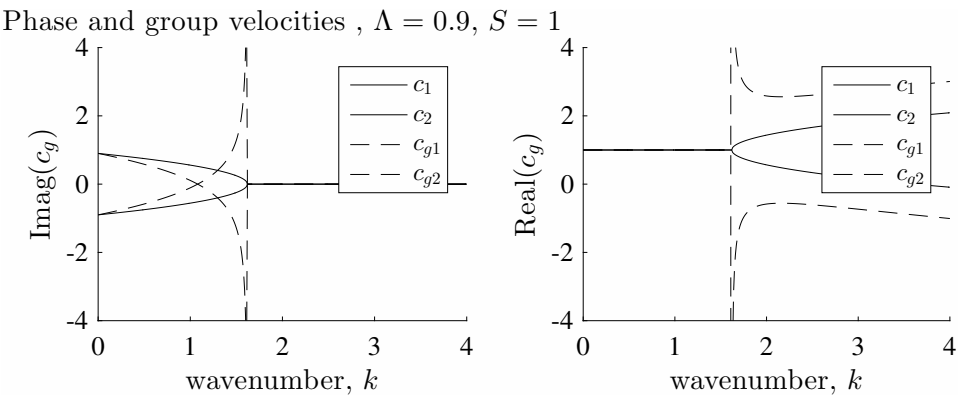

Figure 1.4. The phase velocity (solid lines) and group velocity (dashed lines) as a function of wavenumber, k, for a single shear layer with surface tension. This is a dispersive medium, which means that waves at different wavenumbers travel at different speeds and that the group velocity does not, in general, equal the phase velocity.

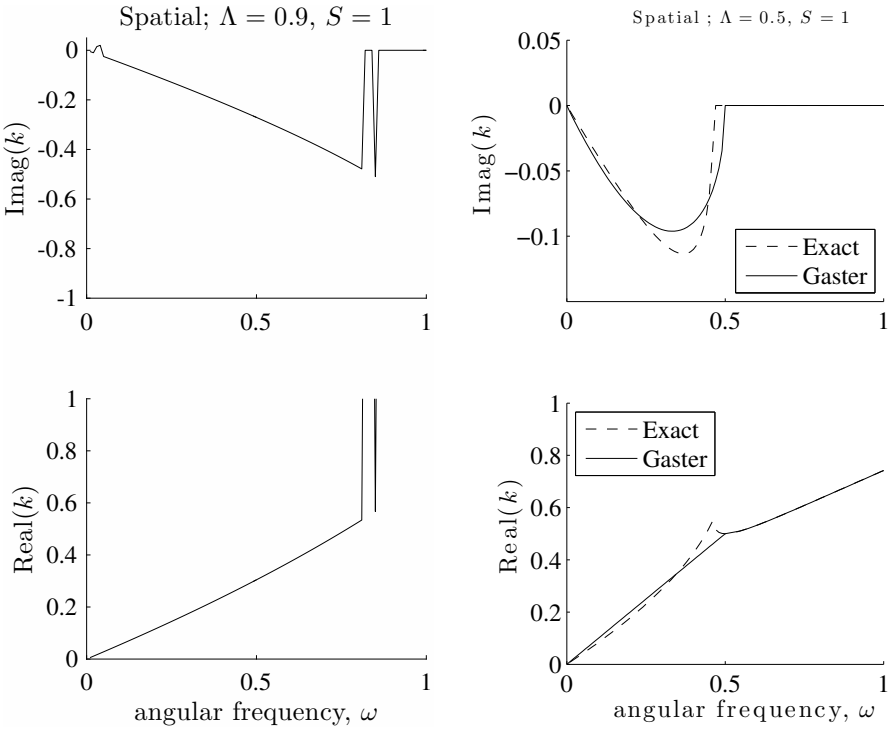

Figure 1.5. The real and imaginary components of k, calculated with a spatial stability analysis, in which ω is constrained to be real. Left: the exact spatial analysis, performed via iteration from a guessed value of k. Right: the approximate spatial analysis from Gaster's transformation compared with the exact spatial analysis, performed via iteration from Gaster's value of k.

problem.

Algorithm `fun_eval_k.m` uses an iterative technique to find k, given ω and an initial guess for k. It uses Matlab's function `fsolve.m`, which tries to set the output, `D`, of `fun_eval_D_loc` to zero by varying its argument `k`. This is where the functions `fun_eval_D_*.m` become useful.

1. Write a script called `script_spatial_001.m` to perform a spatial stability analysis on a single shear layer with $\Lambda = 0.5$ and $S = 1$, as shown in figure 1.5..
2. What has happened at small ω in this figure?
3. What is the most amplified frequency?
4. What happens to the most amplified frequency as Λ increases?

Spatial stability analyses are more difficult to perform than temporal stability analyses and, as we shall see later, have no physical relevance when the flow is absolutely unstable because the transient behaviour overwhelms the signal if the wave with zero group velocity has positive growth rate.

1.10 GASTER'S TRANSFORMATION (1962)

In his 1962 JFM paper [Gaster (1962)], Mike Gaster worked out the relationship between temporal stability and spatial stability (Journal of Fluid Mechanics Vol 14 pp 222–224). The angular frequency and wavenumber pairs from the temporal analysis are labelled $\omega(\mathrm{T})$ and $k(\mathrm{T})$ respectively. The angular frequency and wavenumber pairs from the spatial analysis are labelled $\omega(\mathrm{S})$ and $k(\mathrm{S})$ respectively. He finds that these are approximately related by:

$$k_r(\mathrm{S}) \approx k_r(\mathrm{T}), \tag{1.12}$$

$$\omega_r(\mathrm{S}) \approx \omega_r(\mathrm{T}), \tag{1.13}$$

$$\frac{\omega_i(\mathrm{T})}{k_i(S)} \approx -\frac{\partial \omega_r}{\partial k_r}. \tag{1.14}$$

The final term in (1.14) can be written $-\mathrm{Re}(\mathrm{d}\omega/\mathrm{d}k)$ and is simply the real component of the group velocity.

1. Write a script called `script_spatial_002.m` to compare $k_i(\omega_r)$ calculated with `script_spatial_002.m` with that calculated from Gaster's transformation, as shown in figure 1.5. (right). (You can use Gaster's transformation to improve the initial guess of k for the spatial analysis.)
2. Vary S and Λ to discover when Gaster's transformation works well and when it works badly.

Gaster's transformation begs the question of what happens when the real part of the group velocity is zero. Is the spatial growth rate infinite? Rather than ponder this conundrum now, it is better to progress to a spatio-temporal stability analysis, which will make everything clear.

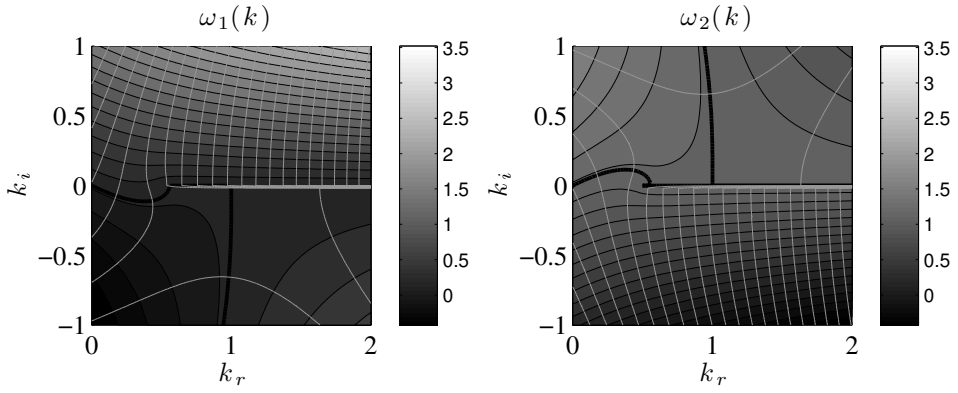

Figure 1.6. Contours of $\omega_i(k)$ (greyscale) and $\omega_r(k)$ (grey lines) for a single shear layer with $\Lambda = 0.9$, $S = 1$. This is a spatio-temporal stability analysis in which both ω and k are complex. The points with $\mathrm{d}\omega/\mathrm{d}k = 0$ can be identified by eye (there is one in each frame). The thick black line is $\omega_i = 0$.

1.11 SPATIO-TEMPORAL STABILITY ANALYSIS

In a spatio-temporal analysis, k and ω are both allowed to be complex numbers. Physically, this means that we consider waves that grow or decay in the streamwise direction and that grow or decay in time. A useful way to picture this is to imagine exciting every wave simultaneously with an impulse at $(x, t) = (0, 0)$ and then observing the evolution of the resulting wavepacket. This is known as an *impulse response* or, equivalently, the *Green's function*. (For the purists: we assume for now that the fluid is incompressible and therefore that all information about the boundary conditions is conveyed instantly to the point of impulse.) The response to any type of forcing can be found from this by convoluting the impulse response with the forcing signal, but we will stick with the impulse response itself because it tells us all that we need to know.

Only some waves are permitted (these are the ones that satisfy the dispersion relation). They propagate away from the point of impulse at different velocities, given by their *group* velocity $\mathrm{d}\omega/\mathrm{d}k$, and grow or decay at different rates, given by their growth rate, ω_i.

If every wave decays in time then the flow is *stable*. If some waves grow in time then the flow is *unstable* and a further distinction is necessary. After a long time, the only wave to remain at the point of impulse is the wave that has zero group velocity. If this wave decays in time, then the impulse response decays to zero at the point of impulse and the flow is called *convectively unstable*. If the wave grows in time, then the impulse response grows to infinity at the point of impulse and the flow is called *absolutely unstable*.

In the next section, we will examine this in more detail. For now, however, we will find the wave with zero group velocity by plotting contours of ω in the complex k-plane.

1. For the single shear layer, write a script called `script_spatemp_001.m` to calculate ω_1 and ω_2 on a grid of complex k with $k_r \in [0, 2]$ and $k_i \in [-1, 1]$. Plot

contours of ω_i and ω_r on the same plot, as in figure 1.6.. (The `stencil` becomes useful here.) Plot the contour $\omega_i = 0$ with double thickness.

2. What do you notice about the relationship between the contours of ω_i and the contours of ω_r?

3. Identify by eye the position where the group velocity is zero. Does it have positive or negative growth rate?

4. Write a function called `fun_eval_dwdk0.m` that uses `fsolve` to converge to this point, given an initial guess, and then displays (ω, k) at this point.

5. Write a script called `script_click.m` that asks the user to click near a point where $\mathrm{d}\omega/\mathrm{d}k = 0$, then converges accurately to that point, then determines whether the flow is absolutely or convectively unstable.

The contours of ω_i and ω_r are always at right angles to each other. Furthermore, the two components of curvature on the surface $\omega_i(k)$ always have opposite sign. This means that points where $\mathrm{d}\omega/\mathrm{d}k = 0$ are *saddle points* of $\omega(k)$. In the long time limit, the impulse response at the point of impulse is dominated by the behaviour of these saddle points. At a saddle point, the values of ω and k are called the *absolute* frequency and wavenumber and are given the symbols ω_0 and k_0.

1. Compare figure 1.3. with figure 1.6. to check that the temporal analysis corresponds to a slice through $\omega(k)$ along the k_r axis.

2. What does the spatial analysis correspond to in figure 1.6.?

3. Explain why a spatial analysis does not work for absolutely unstable flows.

1.11.1 The Briggs-Bers criterion

The aim of this section is to present a more rigorous calculation of the impulse response and to show that some saddle points do not contribute to it. The concepts may be difficult to grasp in a short time, but the main point is summarized at the end.

We want to evaluate

$$\mathbf{u}(x,t) = \int_{-\infty}^{\infty}\int_{-\infty}^{\infty} \hat{\mathbf{u}}(k,\omega)\mathrm{e}^{\mathbf{i}(kx-\omega t)}\,\mathrm{d}\omega\,\mathrm{d}k. \tag{1.15}$$

To evaluate the response at the point of impulse, see [Huerre & Monkewitz (1990)], particularly equation (9), and [Huerre & Monkewitz (2000)], which gives more steps in the calculation. To evaluate the response at every point in space, see [Healey (2006)], particularly figure 11, and [Juniper (2007)], one result from which is shown in figure 1.7..

Figure 1.7. shows contours of the growth rate as a function of group velocity, $(x/t, z/t)$, for all the permitted waves in the impulse response. (It is for varicose perturbations of an unconfined low density jet with $\Lambda = 1/1.1$ and $S = 0.1$.) The impulse response propagates and grows at the point of impulse, $(x/t, z/t) = 0$, so this flow is absolutely unstable. It grows fastest, however, in the downstream direction, $x/t > 0$. The maximum growth

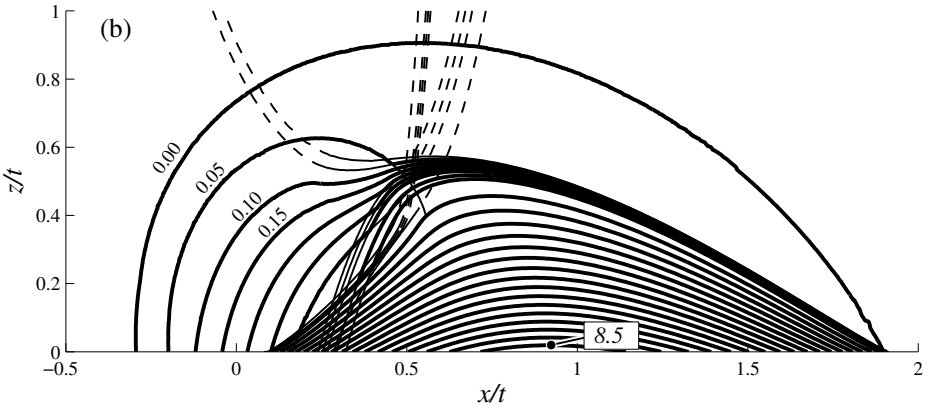

Figure 1.7. This is the impulse response for varicose perturbations of an unconfined low density jet with $\Lambda = 1/1.1$, $S = 0.1$, and finite thickness shear layers. The impulse is at $(x, z) = (0, 0)$ and the resultant waves disperse at their individual group velocities in the x and z directions. The chart plots the growth rate, ω_i, of the wave that dominates along each ray $(x/t, y/t)$, *i.e.* the wave that has group velocity $(x/t, y/t)$. We see that most of the wavepacket propagates and grows downstream (to the right) but that some propagates and grows upstream (to the left). The growth rate at the point of impulse $(x/t, y/t) = (0, 0)$ is positive, which means that this is an absolutely unstable flow.

rate of the impulse response (8.5) is given by the growth rate of the temporal stability analysis because, at this point in the impulse response, $k_i = 0$.

The integral (1.15) can be evaluated by integrating either over ω and then k, or over k and then ω. For these dispersion relations, it easiest to integrate over ω first because, for each k, there are only two permitted values of ω. The integral becomes

$$\mathbf{u}(x,t) = \int_{-\infty}^{\infty} \hat{\mathbf{u}}(k,\omega) \mathrm{e}^{\mathrm{i}(kx-\omega_1(k)t)}\, \mathrm{d}k + \int_{-\infty}^{\infty} \hat{\mathbf{u}}(k,\omega) \mathrm{e}^{\mathrm{i}(kx-\omega_2(k)t)}\, \mathrm{d}k. \qquad (1.16)$$

Initially, the integration path lies on the real k-axis but it can be shifted into the complex k-plane without changing the integral, as long as it is not shifted through branch points or poles (*i.e.* points where $\omega = \pm\infty$). The integral is easiest to evaluate if the integration path is shifted onto lines of constant ω_r because then the phase of $\exp\{\mathrm{i}(kx - \omega t)\}$ remains constant and the integrand does not oscillate as k changes. (Remember that $x = 0$ because we are looking at the point of impulse, so the only term that can oscillate as k varies is $\exp(\mathrm{i}\omega_r(k)t)$.)

In order to pass from $k = -\infty$ to $k = +\infty$, the integration path must cross some (but not all) of the saddle points in the k-plane and, for each of these saddle points, there is only one possible value of ω_r. This means that the integration path must cross these saddle points at this value of ω_r and then change to another value of ω_r at points where ω_i is strongly negative, so that the oscillating contribution to the integral there is negligible.

This is best explained by showing an example. Figure 1.8. shows contours of $\omega_i(k)$ for varicose perturbations of a confined jet flow with $\Lambda = 1$, $S = 1$, $h = 1.3$, $\Sigma = 1$. The integration path needs to pass over two saddle points, s_1 and s_3, in order to pass from

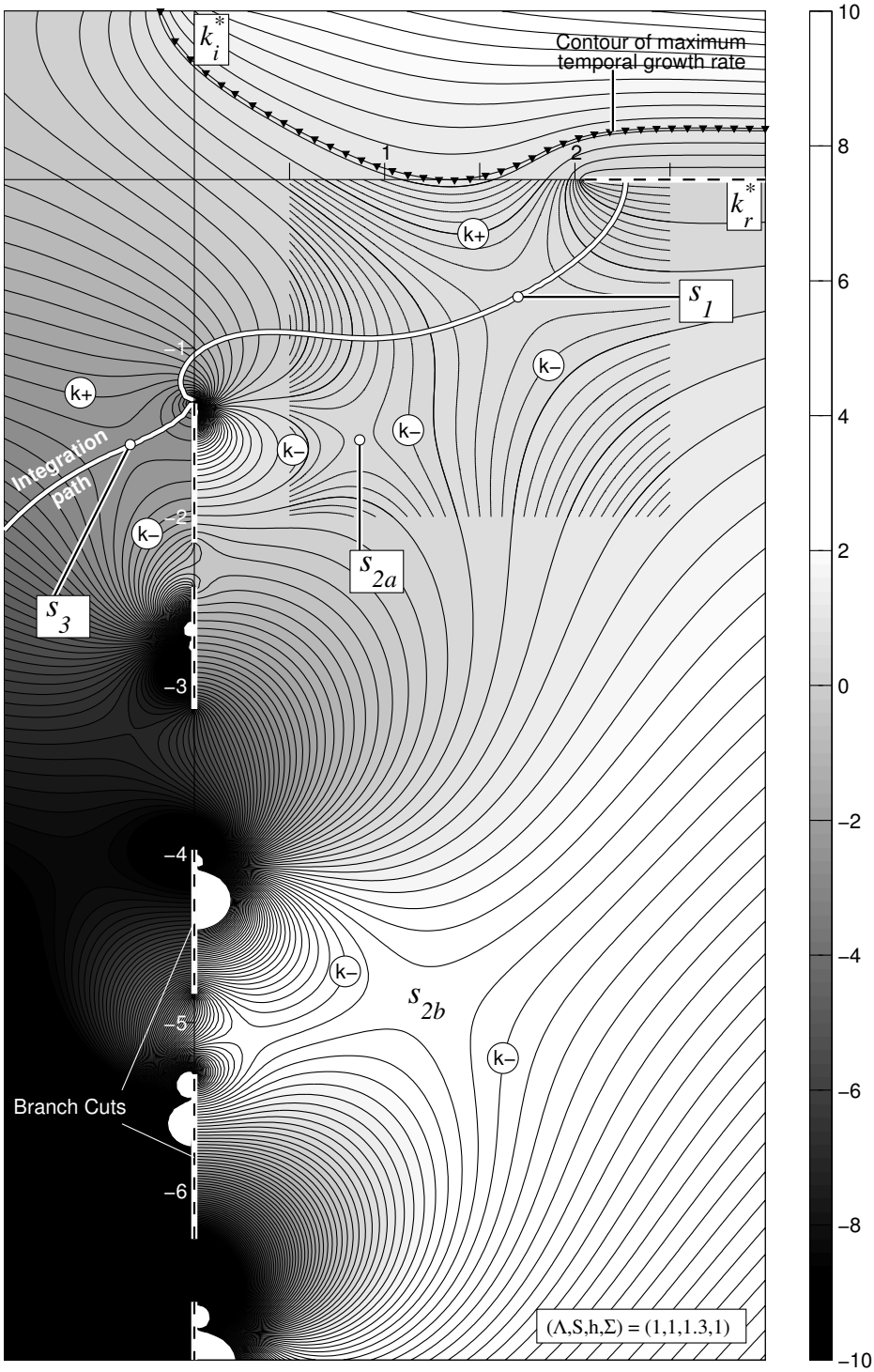

Figure 1.8. Contours of $\omega_i(k)$ for varicose perturbations of a confined jet flow with surface tension, showing the integration path from $k = -\infty$ to $k = +\infty$. The integration path passes over saddle points s_1 and s_3, which means that they contribute to the integral. It does not pass over saddle points s_{2a} or s_{2b}, however, which means that they do not contribute to the integral. This is another way to visualize the Briggs-Bers criterion, which states that a saddle point is only valid if it is pinched between a k^+ and a k^- hill.

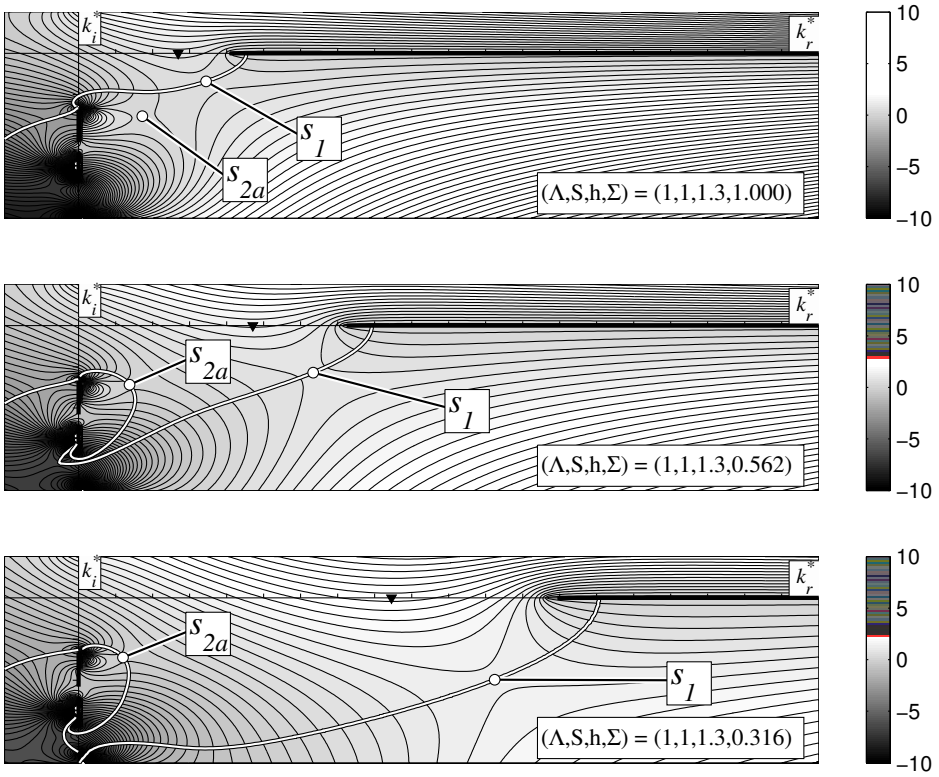

Figure 1.9. Contours of $\omega_i(k)$ for the same flow as figure 1.8. as the surface tension is reduced. This reduction in Σ causes the s_1 saddle to move to lower ω_i and therefore causes the integration path to pass over the s_{2a} saddle point. When the surface tension tends to zero (not shown here) all the s_2 saddle points move onto the integration path.

$k = 0$ to $k = \infty$, but it misses out saddles s_{2a} and s_{2b}. As the surface tension reduces, which is shown in figure 1.9., saddle s_{2a} comes onto the integration contour. As it reduces further, s_{2b} etc. come onto the contour too.

In the long time limit, the dominant contribution to the integral comes from the point on the integration path with highest ω_i, which is always a saddle point. In fact, we already knew that the dominant contribution comes from a saddle point because these are the only points with zero group velocity. But now we know that only some saddle points contribute. You will notice that, if you head directly up the hills (*i.e.* on lines of constant ω_r) on either side of the valid saddle points, one hill goes into the top half k-plane and the other hill goes into the bottom half k-plane. This is the Briggs-Bers criterion. It is another way of stating that the saddle point must lie on the integration path.

1. Write a script called `script_spatemp_002.m` to plot $\omega_1(k)$ for varicose perturbations of a confined jet/wake flow with $\Lambda = 1$, $S = 1$, $h = 1.3$, $\Sigma = 1$. Compare it with figure 1.9..

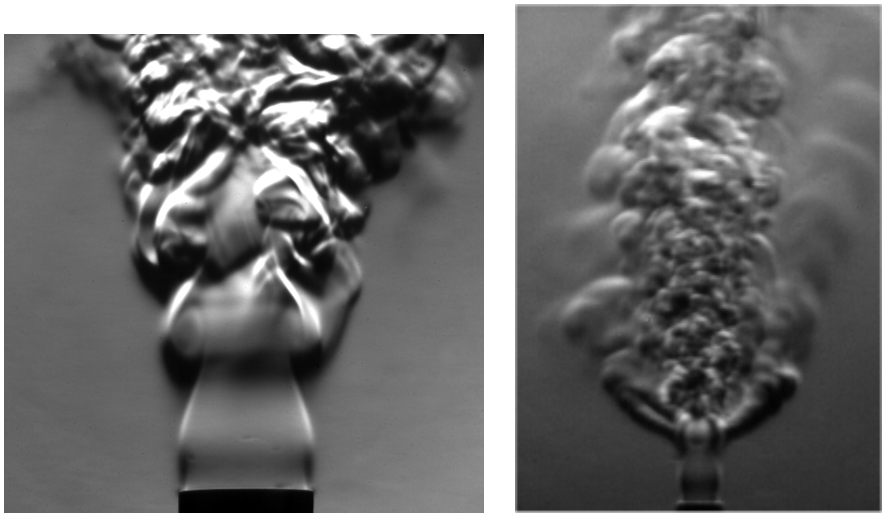

Figure 1.10. Schlieren images of Helium jets (taken by Larry K. B. Li). These show the strong beating that is characteristic of a globally unstable flow. The image on the right also shows side jets, which are a secondary effect of this instability.

2. Investigate how the dominant saddle points change as S decreases, Σ decreases, and h increases. Look particularly at the s_{2a} saddle.

3. Write a script called `script_spatemp_003.m` to repeat this for varicose perturbations of an unconfined jet/wake flow with $\Lambda = 1$, $S = 1$, $\Sigma = 0$. This corresponds to an unconfined jet. Find the s_{2a} saddle point exactly with `script_click.m`

The main point of this section is that only some saddle points contribute to the impulse response and that, in the case of a low density jet with vanishing surface tension, the s_{2a} saddle is one of these.

1.12 LOW DENSITY JETS

Low density round jets are globally unstable because of a sufficiently large region of absolute instability at their base. Two examples are shown in figure 1.10.. Although these jets are round, the dispersion relation `fun_eval_*_uncon_jetwake_var.m` can model them reasonably accurately. In these exercises, we will map the absolutely unstable region of a low density jet in (Λ, S)-space.

1. Write a function called `fun_eval_w0i`, which takes in a value of Λ and returns the growth rate, ω_{0i}, of the saddle point. The input arguments will have to be `(param,k_init,L,tol)`, where `param` contains all the parameters except `L`, `k_init` is an initial guess for the wavenumber of the saddle point, and `tol` is the tolerance required for `fun_eval_dwdk0.m`.

2. Embed `fun_eval_w0i` within another function called `fun_eval_L`, which uses `fsolve` to reduce ω_{0i} to zero by changing `L`.

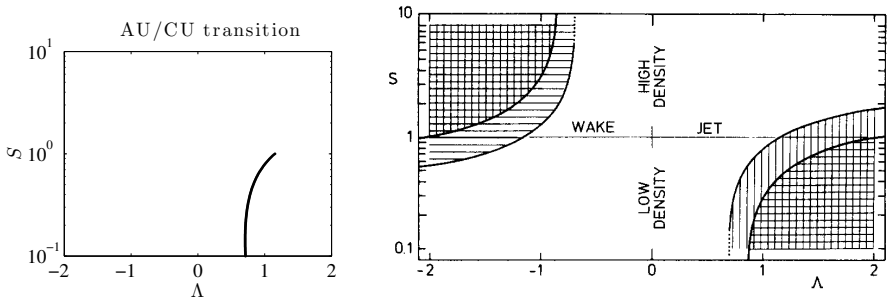

Figure 1.11. Absolute / Convective transition lines for unconfined planar jets and wakes as a function of velocity ratio Λ and density ratio S. Left: created with `script_SL_var_001.m` (currently incomplete). Right: from [Yu & Monkewitz (1990)].

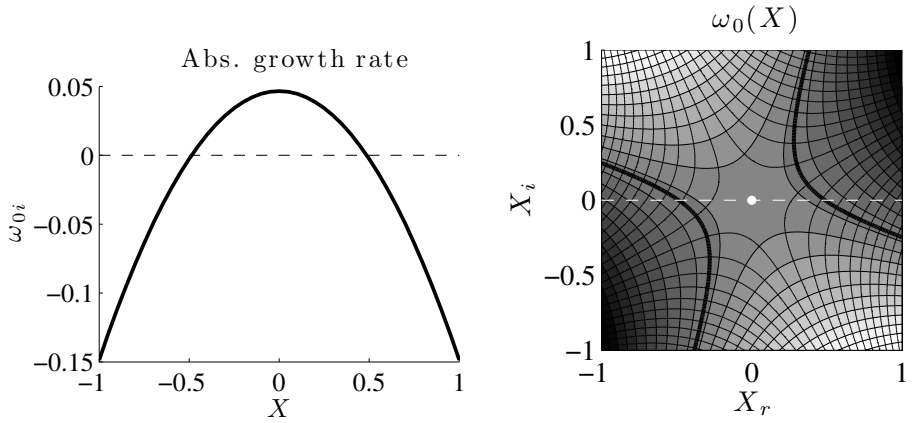

Figure 1.12. The absolute growth rate ω_{0i} as a function of the long streamwise distance, X. Left: as calculated from the saddle points of the base flow. Right: after interpolation with a second order polynomial and analytical continuation into the complex X-plane.

3. Write a script called `script_SL_var`, which varies S between 0.1 and 1 and plots the values of Λ for which $\omega_{0i} = 0$, as in figure 1.11. (left).

4. Write a script called `script_SL_var_002`, which finds the absolutely unstable regions for unconfined jets and wakes within the range $S \in [0.1, 10]$ and $\Lambda \in [-2, 2]$. Compare your results with those from [Yu & Monkewitz (1990)], which are shown in figure 1.11. (right).

1.12.1 Calculating the linear global mode frequency

For flows that evolve slowly in the streamwise direction it is possible to combine the slices in order to work out the global mode growth rate. The details are explained in [Huerre & Monkewitz (1990)] and in more detail in [Monkewitz, Huerre & Chomaz (1993)].

The first stage of this analysis is to calculate the absolute frequency ω_0 as a function of the downstream distance, X. (This is a function of the long lengthscale, X, rather than the short lengthscale, x). To do this, we assume that $\omega_0(X)$ can be continued analytically into the complex X-plane. If $\omega_0(X)$ varies slowly in the X-direction and if $\omega_{0i}(X)$ reaches a maximum within the domain being considered then $\omega_0(X)$ will have a saddle point at some complex value of X close to the X_r axis. The value of ω_0 at this saddle point gives the frequency and growth rate of the linear global mode, ω_g.

It is not possible to continue $\omega_0(X)$ itself into the complex X-plane because we only have information on the X_r axis. Instead, we interpolate a polynomial through $\omega_0(X)$ and then continue this polynomial into the complex X-plane. Then we look for saddle points of this polynomial.

1. Write a script called `script_w0X_001.m` which calculates $\omega_0(X)$ and $k_0(X)$ for varicose perturbations of a uniform density jet in which $\Lambda = 1.2 - 0.2X^2$ and $X \in [-1, 1]$, as in figure 1.12. (left). (This is a crude model of the flow around a Rankine body.) Save `param`, `L`, `X`, `w0`, and `k0` to file `script_w0X_001.mat`
2. Write a script called `script_w0X_002.mat` which uses `polyfit` to fit a second order polynomial through $\omega_0(X)$ and plots contours of ω_{0i} and ω_{0r} in the complex X-plane for $X_r \in [-1, 1]$ and $X_i \in [-1, 1]$, as in figure 1.12. (right) Find the position of the saddle point, (ω_g, X_g). Save `wg`, and `Xg` to file `script_w0X_002.mat`.
3. Try out different models for $\Lambda(X)$ (*e.g.* $\Lambda = 1.3 - 0.1 * X + 0.1X^3 - 0.3X^4$).

1.13 CALCULATING THE LINEAR GLOBAL MODE SHAPE

In order to calculate the linear global mode shape, the response of the whole flow must be calculated at the frequency and growth rate of the linear global mode, ω_g. Each slice is forced at ω_g and its streamwise wavenumber and growth rate, k, are calculated. For each ω_g there are usually an infinite number of values of k. We need to choose the two that pass closest to the saddle point of $\omega_0(k)$ at the X-position of the saddle point $\omega_0(X)$. The downstream-travelling wave is labelled k^+ and the upstream-travelling wave is labelled k^-.

The corresponding global mode shape is calculated by integrating

$$\mathbf{u}(x, z, t) \sim A_0(X)\hat{\mathbf{u}}^{\pm}(z; X) \exp\left(\frac{\mathrm{i}}{\epsilon}\int_0^X k^{\pm}(X'; \omega)\, \mathrm{d}X' - \omega_g t\right), \tag{1.17}$$

where, at the X-position of each slice, k^+ is the local wavenumber downstream of X_s, k^- is the local wavenumber upstream of X_s, and $\hat{\mathbf{u}}^{\pm}(z; X)$ is the corresponding eigenfunction. The slowly-varying amplitude, $A_0(X)$, is usually assumed to be uniform because the influence of this assumption is much smaller than the influence of the inaccuracies in $k^{\pm}$.

Unfortunately, the dispersion relations studied here correspond to cases that are never stable. (They are either convectively unstable or absolutely unstable). This means that the global mode grows without limit in the x-direction, which is not physical. This means

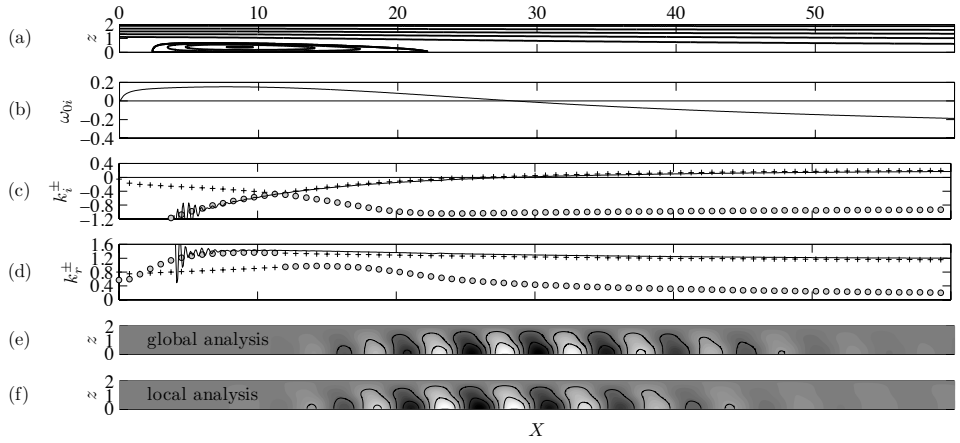

Figure 1.13. The base flow (a), local stability properties (b–d) and global modes (e–f) of a confined planar wake with $h = 1$, $\Lambda^{-1} = -1.2$, $Re = 400$ and free slip boundaries; (a) streamlines; (b) absolute growth rate, ω_{0i}; (c) spatial growthrates, k_i^+ (+) and k_i^- (∘), calculated with the local analysis, compared with k_i (–) extracted from the global analysis (the latter is noisy at the upstream end because the amplitude is small); (d) as for (c) but for the real spatial wavenumbers, $k_r^\pm$; (e) $\hat{v}(x,z)$ of the first eigenmode calculated with the global analysis; (f) $\hat{v}(x,z)$ of the first eigenmode calculated with the local analysis. From [Juniper, Tammisola & Lundell (2011)].

that we have come as far as we can with these simple models. Nevertheless, if you want to continue the analysis with different dispersion relations, the following exercises explain how to calculate the x-dependence of the global mode by integrating (1.17).

1. Starting from the slice at the axial location of the saddle point $\omega_0(X)$, write a script called `script_kX_001.m` that finds two different values of $k(\omega_g)$ on either side of the saddle point at k_0. Save `kp` and `km` to file `script_kX_001.mat`.

2. Starting from the values of k^+ and k^- at this slice, write a script called `script_kX_002.m` that iterates through all the slices to find $k^+(X)$ and $k^-(X)$. Save `X`, `ind`, `kpX` and `kmX` to file `script_kX_001.mat`.

3. Write a script called `script_uX_001.m` that integrates (1.17) to find the x-dependence of the global mode.

Figure 1.13. shows a comparison between a global mode calculated with a 2D global analysis, frame (f), with that from a local analysis, frame (g), taken from [Juniper, Tammisola & Lundell (2011)]. These are for a viscous wake flow, which becomes stable at $x \approx 30$. The two global modes are remarkably similar. The main difference arises from the fact that the local analysis slightly over-predicts the growth rate of the linear global mode. If this is corrected, the two mode shapes are nearly identical.

Local stability analysis is only strictly valid when the flow is parallel or weakly non-parallel. Nevertheless, it can be a useful diagnostic tool for strongly non-parallel flows. In figure 1.14., for example, we see that the vortex breakdown bubble has two regions of absolute instability: one in the bubble itself and one in the wake behind it. Both of these regions can support a global mode. Indeed, this flow seems to behave as if it is being forced

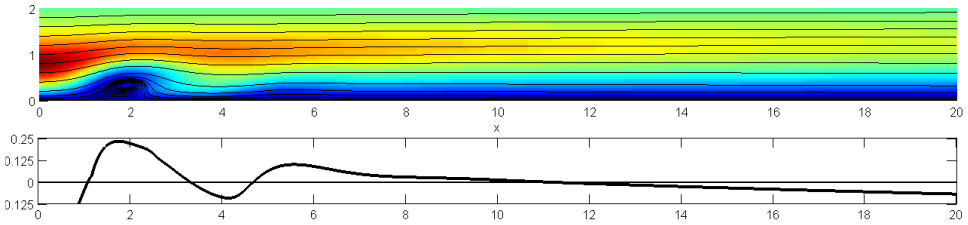

Figure 1.14. Top: streamlines (black) and azimuthal velocity (colours) for a vortex breakdown bubble at $Re = 400$. Bottom: absolute growth rate, $\omega_{0i}(X)$. From Qadri, Mistry & Juniper (2012)

by two coupled oscillators.

Finally, local stability analyses can also predict the frequency of saturated nonlinear global modes; [Pier, Huerre & Chomaz].

REFERENCES

Drazin & Reid (1981). DRAZIN, P. & REID, W. 1981 Hydrodynamic Stability. Cambridge University Press.

Gaster (1962). GASTER, M. 1962 A note on the relation between temporally-increasing and spatially-increasing disturbances in hydrodynamic stability *J. Fluid Mech.* **14**, 222–224.

Huerre & Monkewitz (1990). HUERRE, P. & MONKEWITZ, P. A. 1990 Local and global instabilities in spatially developing flows *Ann. Rev. Fluid Mech.* **22**, 473–537.

Huerre & Monkewitz (2000). HUERRE, P. & MONKEWITZ, P. A. 2000 Open shear flow instabilities. In *Perspectives in fluid dynamics : a collective introduction to current research* (eds. G. K. Batchelor, H. K. Moffat & M. G. Worster) C.U.P.

Healey (2006). HEALEY, J. J. 2006 A new convective instability of the rotating-disk boundary layer with growth normal to the plate *J. Fluid Mech.* **560**, 279–310.

Juniper (2007). JUNIPER, M. P. 2007 The full impulse response of two-dimensional shear flows and implications for confinement *J. Fluid Mech.* **590**, 163–185.

Juniper, Tammisola & Lundell (2011). JUNIPER, M. P., TAMMISOLA, O. & LUNDELL, F. 2011 The local and global stability of confined planar wakes at intermediate Reynolds number *J. Fluid Mech.* in print

Monkewitz, Huerre & Chomaz (1993). MONKEWITZ, P. A., HUERRE, P., & CHOMAZ, J-M. 1993 Global linear stability analysis of weakly non-parallel shear flows *J. Fluid Mech.* **251**, 1–20.

Pier, Huerre & Chomaz. PIER, B., HUERRE, P. & CHOMAZ, J-M 2001 Bifurcation to fully nonlinear synchronized structures in slowly varying media *Physica D* **148**, 49–96.

Rayleigh (1896). RAYLEIGH, J.W.S. 1898 The Theory of Sound, Vol 2, Dover.

Rees & Juniper (2009). REES, S. J. & JUNIPER, M. P. 2009 The effect of surface tension on the stability of unconfined and confined planar jets and wakes *J. Fluid Mech.* **633**, 71–97.

Strogatz (2001). STROGATZ, S. H. 2001 Nonlinear Dynamics And Chaos, Westview Press.

Yu & Monkewitz (1990). YU, M-H. & MONKEWITZ, P. A. 1990 The effect of nonuniform density on the absolute instability of two-dimensional inertial jets and wakes *Phys. Fluids A* **2**(7), 1175–1181.